nature communications

Article

https://doi.org/10.1038/s41467-024-50974-x

Directional long-distance electron transfer from reduced to oxidized zones in the subsurface

Received: 1 April 2024

Accepted: 26 July 2024

Published online: 03 August 2024

Check for updates

Yanting Zhang[1], Man Tong[1,2], Yuxi Lu[1], Fengyi Zhao[1], Peng Zhang[1], Zhenchen Wan[1], Ping Li[1,2], Songhu Yuan[1,2] ✉, Yanxin Wang[1,2] & Andreas Kappler[3,4]

Electron transfer (ET) is the fundamental redox process of life and element cycling. The ET distance is normally as short as nanometers or micrometers in the subsurface. However, the redox gradient in the subsurface is as long as centimeters or even meters. This gap triggers an intriguing question whether directional long-distance ET from reduced to oxidized zones exists along the redox gradient. By using electron-donating capacity variation as a proxy of ET, we show that ET can last over 10 cm along the redox gradient in sediment columns, through a directional long-distance ET chain from reduced to oxidized zones constituted by a series of short-distance electron hopping reactions. Microbial and chemical processes synergistically mediate the long-distance ET chain, with an estimated flux of 6.73 μmol e^-/cm^2 per day. This directional long-distance ET represents an overlooked but important "remote" source of electrons for local biogeochemical and environmental processes.

Electron transfer (ET) is the fundamental redox process for life on Earth. In the subsurface, ET over different distances is central to most biogeochemical processes such as element cycling, greenhouse gas emission, and the fate of contaminants in both natural and engineered systems[1–3]. ET between connected redox couples, such as mineral-solution[4], microbe-solution[5], and microbe-mineral interfaces[6], is apparently nondirectional, short-distance in the scale of nanometers to micrometers, and constrained to the local zone. For a long-distance ET over centimeters or longer, electron shuttling by conductors like pyrite[7] and magnetite[8] has been reported, and long-distance bridging cable bacteria[9] has been discovered in the recent decade. These ET processes are significant only in the scenario where conductors and/or cable bacteria are present. Recent studies demonstrated that cycling of natural organic matter (NOM) between reduced and oxidized forms in agar-solidified systems can enable ET over a distance of 2 cm between microbes and ferrihydrite[10]. Inspecting subsurface redox profiles, we can find that the redox gradient is directional and long-distance. The reduction potential generally decreases from the surface for O_2 (or nitrate) reduction to different depths below the surface for reduction of iron(III) (or other oxidants)[2,11] (Fig. 1), reaching the distance of centimeters to meters or even longer. Thus, an intriguing question arises regarding whether directional ET exists along the long-distance redox gradient in the subsurface.

Here we hypothesize that a directional long-distance ET chain from reduced to oxidized zones exists along the redox gradient in the subsurface. This ET chain is composed of a directional series of short-distance primary ET processes from low to high reduction potentials (Fig. 1). For example, ET can occur from Fe(II) (or reduced NOM) to neighboring Fe(III) (or oxidized NOM) with the generation of neighboring Fe(II) (or reduced NOM), and this cycle proceeds directionally along the redox gradient. Previous studies have substantiated the existence of short-distance ET via electron hopping between solutes (i.e., dissolved Fe(II) and NOM) and minerals (i.e., Fe- and Mn-bearing minerals)[12–14], between minerals and minerals[15], between solutes and

[1]State Key Laboratory of Biogeology and Environmental Geology, China University of Geosciences, Wuhan, China. [2]Hubei Key Laboratory of Yangtze Catchment Environmental Aquatic Science, School of Environmental Studies, China University of Geosciences, Wuhan, China. [3]Department of Geosciences, University of Tübingen, Tübingen, Germany. [4]Cluster of Excellence: EXC 2124: Controlling Microbes to Fight Infection, Tübingen, Germany.
✉e-mail: yuansonghu622@cug.edu.cn

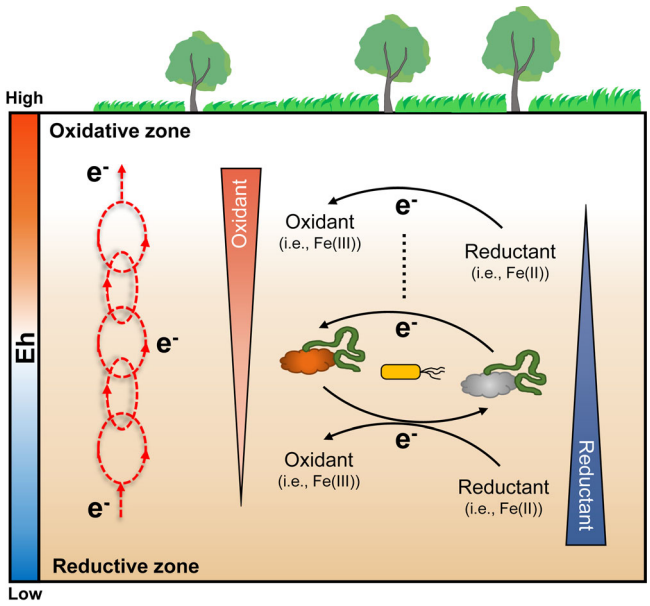

Fig. 1 | Conceptual model of directional long-distance ET chain along subsurface redox gradient. The red circles in the left conceptualize the series of short-distance ET (electron transfer) between connected redox couples from low to high reduction potentials. The redox couples in the right present the biological and chemical mechanisms for the ET.

solutes (i.e., reduced and oxidized NOM)[16], as well as through bulk crystal conduction within semiconductive minerals[4]. The short-distance ET between microbes and other non-dissolved species has been acknowledged through extracellular ET[6,17]. These short-distance abiotic and biotic electron hopping reactions are ubiquitous in the subsurface, which is supposed to constitute the primary units of the proposed directional long-distance ET chain.

In this study, we tested the above hypothesis by measuring the temporal variation of sediment electron-donating capacity (EDC) along a redox gradient in column experiments. EDC represents the moles of electrons that can be released from a specific redox-active substance at a given potential[18]. We show that sediment EDC increases in the oxidized zones and decreases in the reduced zones, with the involvement of a directional long-distance ET chain at the scale of ~10 cm. This ET chain proceeds synergistically through biotic and abiotic mechanisms due to microbes and redox-active species like Fe and NOM. Our results estimate an ET flux of 6.73 μmol e^-/cm^2 per day from the deep reduced zone to the surface oxidized zone. Our finding implies that environmental habitats can be "wired" over long distances by the widespread long-distance ET chain between different zones with a redox gradient in the subsurface.

Results

Directional long-distance ET along a sediment redox gradient

Mediated electrochemical oxidation (MEO) was used to measure EDC as it has been successfully applied to quantify the ET in geochemical and some biogeochemical processes[19–21]. Consequently, the variation in EDC values (ΔEDC) could be used as a proxy to reflect ET in the sediments from one zone to another zone. The rationality was justified by the supplementary experiments (Supplementary Section 3). We explored the long-distance ET by measuring ΔEDC in 10.6-cm long columns filled with different textures (clay loam (clay loam-1 described in Supplementary Section 1), silt loam and sand loam) of anoxic sediments (Fig. 2a). The redox gradient was created by filling oxidized (E_h = +420 to +580 mV) and reduced (E_h = −137 to −380 mV) sediments in the upper and bottom halves of the column, respectively (Supplementary Table 1). For the clay loam sediment, ΔEDC values within 24 d at 1.3 cm above the oxidized/reduced interface increased gradually to 14.8 μmol e^-/g; at −1.3 cm below the interface decreased to −14.2 μmol e^-/g; and their sum at around 0 reveals a nearly symmetric variation in the oxidized and reduced halves (Fig. 2b). Nearly symmetric ΔEDC variations at different locations of the oxidized and reduced halves were also observed at different time, with the variation decreased from the zones near interface (1.3 and −1.3 cm) to the two ends (5.3 and −5.3 cm) (Fig. 2c). Similar observations were obtained for silt and sand loam sediments, with the symmetric ΔEDC variation less pronounced for sand loam sediment (Fig. 2d, e and Supplementary Fig. 9).

As EDC was measured by the chemical reaction between probe and sediment, one likely influence on its usage comes from the localized microbial processes which could transform the reduced species that cannot be measured by MEO to those that can be measured. We evaluated the potential influence of NOM which cannot react with the probe but can be oxidized by microbes (Supplementary Section 3). Results show that this contribution was of minor importance relative to the observed ΔEDC for the above clay loam sediment. Consequently, the symmetric ΔEDC variation suggests that electrons were donated from the reduced sediments in the bottom half and were accepted by the oxidized sediments in the upper half, and thus a 10.6 cm-distance of directional ET occurred from low to high reduction potentials within 24 d.

Roles of microbial and chemical processes in long-distance ET

To unravel the mechanisms controlling the directional long-distance ET, we evaluated the roles of microbial and chemical processes by sterilizing the sediments with different intensities (Supplementary Section 2). For the untreated, $HgCl_2$ + NaN_3 treated and autoclaved sediments, RNA-based 16S rRNA gene abundance decreased sequentially (details in Methods and Supplementary Fig. 3). In order to quantitatively compare the long-distance ET, we calculated the ET flux across the oxidized/reduced interface in the sediment columns by summing ΔEDC in the whole reduced half (Supplementary Section 5). The ET flux within 24 d decreased from 151.8 to 95.8 and 68.0 μmol e^-/cm^2 when the sterilization intensity increased from "Untreated" to "$HgCl_2$ + NaN_3" and "Autoclaved" treatments (Fig. 3a). This dependence corroborates the important role of microbial process in the long-distance ET. To completely inhibit microbial activity, gamma radiation ("Gamma-rays", Supplementary Section 2) was further employed as an abiotic control[22]. The ET flux in the "Gamma-rays" column further decreased to 19.1 μmol e^-/cm^2 within 24 d (Fig. 3a), which further highlights the importance of the microbial process. Whereas, the role of chemical processes could be underestimated to some extent as "Gamma-rays" and "Autoclaved" treatments may induce crystallization of Fe (oxyhydr) oxides and/or an increase of dissolved organic carbon (DOC) (Supplementary Fig. 4)[23], and the chemical processes associated with the microbial processes (i.e., synergist processes) could also be attenuated.

Importance of physical contact between reduced and oxidized sediments

To justify whether electrons were transported from the bottom reduced to the upper oxidized sediments in the columns, we measured the ET flux in the control columns with different fillings in the reduced/oxidized interface. A 2-cm thickness of quartz sand was first intercalated in the interface, which physically separated the reduced and oxidized sediments (Supplementary Fig. 2b). In this column, ΔEDC within 24 d at oxidized and reduced sediments became minimal (≤5.5 μmol e^-/g) (Fig. 4a and Supplementary Fig. 13a). As the texture of quartz sand is different from the sediments filled in the columns, we instead intercalated a 1-cm thickness of sterilized oxidized (or reduced) sediment just above (or below) the interface (Supplementary Section 2 and Supplementary Fig. 2c). In this case, the sediment has the same texture but lower microbial activity. Results show that the ΔEDC

https://doi.org/10.1038/s41467-024-50974-x

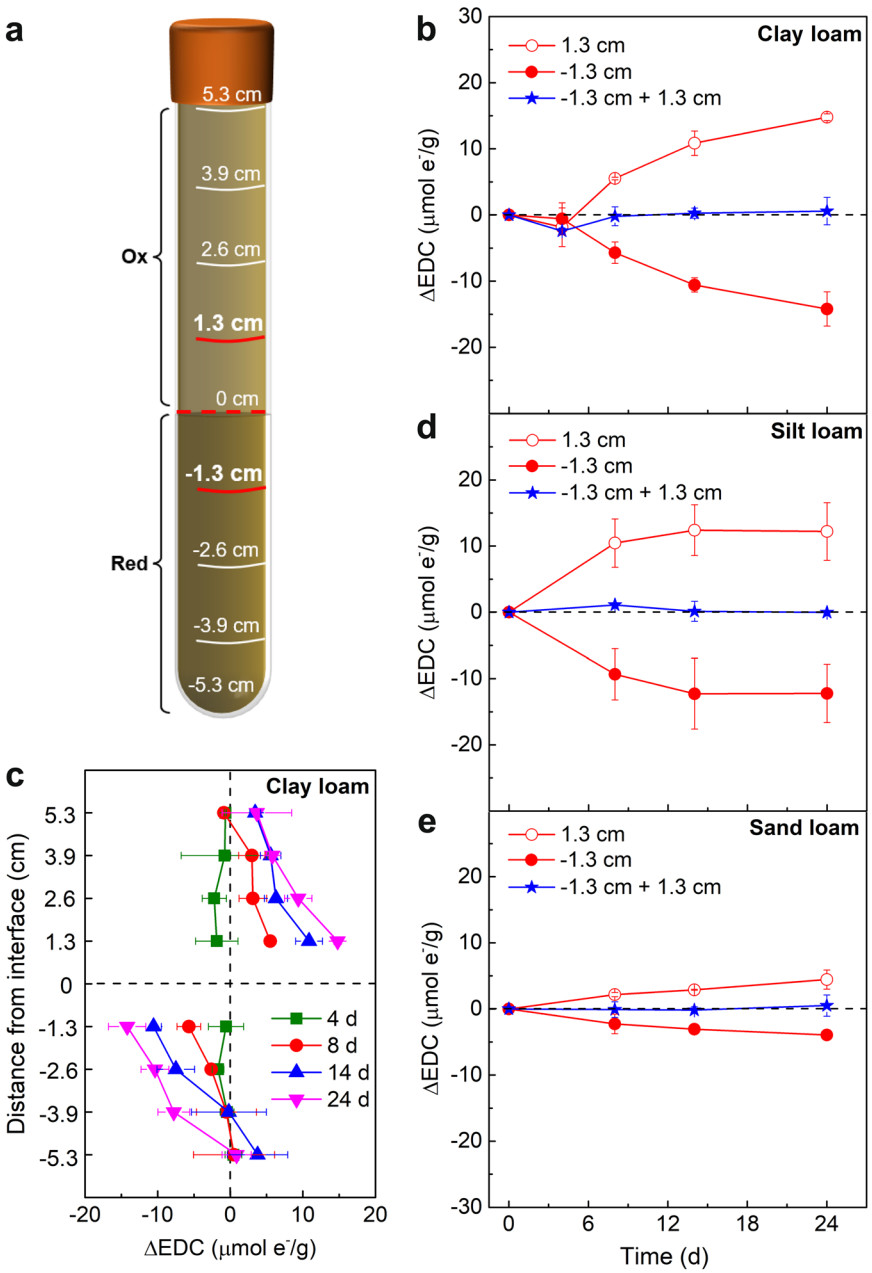

Fig. 2 | Long-distance ET in different textures of anoxic sediment columns. **a** Schematic of a column filled with oxidized ("Ox") and reduced ("Red") sediments in the upper and bottom halves, respectively. **b** Temporal variation of ΔEDC near the oxidized/reduced interface (locations at 1.3 and −1.3 cm) and **c** spatial variation of ΔEDC in the clay loam columns at different times. Temporal variation of ΔEDC near the oxidized/reduced interface (locations at 1.3 and −1.3 cm) in the **d** silt loam and **e** sand loam columns. ΔEDC was calculated by the value difference between sampling and initial time. The initial EDC values for the oxidized halves in clay loam, silt loam, and sand loam were 18.5, 21.2, and 2.5 μmol e^-/g, respectively, and for the reduced halves were 48.3, 55.7, and 20.4 μmol e^-/g, respectively (Table 1). The ΔEDC values for "−1.3 cm + 1.3 cm" were calculated by the sum of values at locations at 1.3 and −1.3 cm in different textures of sediment columns. Note that all the sediments were immersed in 250 mg/L $HgCl_2$ and 500 mg/L NaN_3 prior to filling in order to moderately inhibit microbial activity. Error bars represent standard deviations of duplicate columns (mean ± standard error, $n = 2$, independent replicates).

values near the interface decreased largely relative to the same column without intercalation (Figs. 2b, 4b, c and Supplementary Fig. 14a). The water contents in all the locations did not vary noticeably (<2%) during 24 d, indicating that convection and diffusion was weak in the clay loam sediments. The large decrease in ΔEDC reflected that the redox-active solutes could not diffuse across a distance of 1–2 cm. Collectively, these control columns corroborate that physical contact between oxidized and reduced sediments could be essential for the long-distance ET, microbial activity, especially in the interface plays an important role, and the diffusion of redox-active solutes in sediment porewater did not contribute significantly at the centimeter scale.

Effects of extreme pH and low temperature

As pH and temperature are important parameters in the subsurface that largely impact microbial processes[11,24,25], we further observed the response of long-distance ET to extreme pH and temperature conditions. The sediment columns were acidified to pH ~4 ("Acid perturbation") or alkalized to pH ~12 ("Base perturbation"), or were maintained

https://doi.org/10.1038/s41467-024-50974-x

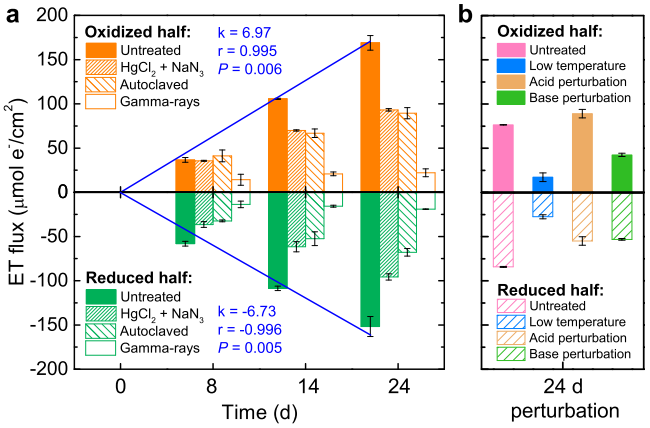

Fig. 3 | Roles of microbial and chemical perturbations in the long-distance ET in sediment columns. a Temporal variation of ET flux for the oxidized and reduced halves in the columns with different sterilized sediments, and linear correlations of ET flux with time in the untreated columns (blue lines). Calculation of ET flux is described in Supplementary Section 1. **b** Variation of ET flux for the oxidized and reduced halves in the columns under low-temperature, acidic, or basic conditions. Clay loam sediments (Table 1) were filled into the columns as described in Methods. Prior to filling, the sediments were treated by immersing in 250 mg/L $HgCl_2$ and 500 mg/L NaN_3 ("$HgCl_2$ + NaN_3"), autoclaving for 20 min ("Autoclaved") and gamma radiation for a dose of 52 ± 5.2 kGy ("Gamma-rays") (Supplementary Section 2). "Low temperature" means the sediment column was kept at low temperature (−20 °C). "Acid perturbation" (or "Base perturbation") means that the initial sediment pH was acidified to ~4 (or alkalized to ~12). The significances of correlation in **a** were analyzed through Pearson correlation (one-sided). Error bars represent standard deviations of duplicate columns (mean ± standard error, $n = 2$, independent replicates).

at −20 °C ("Low temperature") (Supplementary Section 6). We surprisingly found that the ET flux in these columns only decreased by 34.8–67.5% relative to those in the untreated column (reduced halves in Fig. 3b). For microbial processes, both temperature and pH are known to influence the structure and functions of soil microbial communities[26,27]. For example, it was reported that the average metabolic rate for prokaryotes in Siberian permafrost and South Pole ice and snow was decreased by about 3 orders of magnitude when the temperature decreased from +16 to −20 °C[28]; and when the pH decreased from 7.0 to 4.5, the bacterial growth in a silt loam soil was decreased by 80%[29]. To further evaluate the microbial activity due to these perturbations, the abundance of RNA-based 16S rRNA genes was quantified in the sediments. The abundance was decreased by 3 orders of magnitude for temperature perturbation within 24 h (Supplementary Fig. 3), which was close to the reported decrease[28]. For pH perturbations, the abundance was decreased by 2 orders of magnitude (Supplementary Fig. 3), which suggests a weaker microbial activity than in the previous study[29]. Whereas for chemical processes, acidification can dissolve Fe species, and alkalization can also dissolve NOM. So, the concentrations of dissolved redox-active components in sediment porewaters could be increased under extreme pH conditions. Thus, the decrease of ET flux was much less significant than that for microbial activity[28,29], which supports the synergistic effect of microbial and chemical processes. As a result, we infer that the role of chemical processes under extremely acidic/alkaline and cold conditions could become more pronounced compared with the mild conditions favorable for microbial processes.

Enhancement by air exposure due to an elevated redox gradient

As an important driving force for electron transfer, redox gradients exhibit temporal and spatial variations in the subsurface because of various amounts of reduced and oxidized substances[1,11,30]. We further investigated the impact of the redox gradient on long-distance ET. In detail, the top of oxidized sediments in the upper half of the column was uncovered and exposed to air to maintain the redox gradient. We saw that the ΔEDC values at 1.3 cm above the redox interface were always close to 0 within 24 d, and at 1.3 cm below the interface decreased to −17.55 μmol e^-/g (Fig. 4d). The ET flux in the O_2-perturbated column within 24 d was 133.9 μmol e^-/cm^2 (Supplementary Fig. 20), which is 1.4-fold of the ET flux in the reference column ("$HgCl_2$ + NaN_3" column in Fig. 3a). During 24 d incubation, the water content for upper oxidized sediments was only decreased 1.02–2.35% (Supplementary Fig. 20b), suggesting an insignificant contribution of air penetration. As a result, the electrons transported to the upper oxidized sediment can be further consumed by O_2 at the water-air interface, which maintains a high redox gradient and facilitates the ET from the bottom reduced sediments. We, therefore, conclude that an elevated redox gradient can promote long-distance ET. This scenario is common to the field soil/sediment profile, in which the surface is always exposed to air or oxygenated water while the bottom remains reduced. For example, O_2 is rich in the overlying water of aquatic ecosystems, flooded soils, and sediments[31,32]. In the subsurface, while the groundwater table is lower, atmospheric O_2 can be present in the unsaturated pore spaces above the water table[30].

Discussion

The above results corroborate that directional long-distance ET occurred along the redox gradient in the sediment columns, and microbial and chemical processes contributed synergistically. As the short-distance ET has been previously described at the interfaces of solute, mineral, and microbe, both individually and collectively[11,15,33], here we only discuss the mechanisms of directional long-distance ET. The likely mechanisms include (1) electrons shuttled by conductors, (2) electrons shuttled by cable bacteria, (3) diffusion of reduced species from the reduced to the oxidized zone; (4) electron hopping between redox couples in porewater, and (5) a directional series of many types of short-distance ET units as we hypothesized (Fig. 1). The 1st and 2nd mechanisms did not contribute to a significant extent, because conductors like pyrite and magnetite were not identified by XRD (Supplementary Figs. 1 and 16), and cable bacteria were not detected by 16S rRNA microbial community analysis (Supplementary Fig. 15). The 3rd mechanism could be of minor importance, as supported by the essential role of physical contact (Fig. 4a–c). For the 4th mechanism, we measured the redox properties of sediment porewaters in the columns. As we cannot collect the required volume of porewaters, the properties were approximately estimated from water-extracted values. For the 3 types of sediments investigated, the initial EDC for the pore waters in the reduced sediments ranged between 0.3 and 5.7 mmol e^-/L, and the initial EAC for the pore waters in the oxidized sediments ranged from 2.1 to 20.4 mmol e^-/L (Supplementary Table 2). To explore the likelihood of electron hopping, the concentrations of redox-active species in the pore waters for the "Gamma-ray" columns were determined. The DOC concentrations, dissolved total Fe concentrations, EDC, and EAC values ranged from 7.9 to 18.0 mM, 0.6 to 2.4 mM, 0.1 to 3.5 mmol e^-/L, and 2.0–26.0 mmol e^-/L, respectively (Supplementary Table 3). As electron hopping between reduced and oxidized NOM can mediate ET over the distance of centimeters from low to high reduction potential[34], we conclude that electron hopping between the reduced and oxidized forms of dissolved redox-active species (i.e., DOC, Fe, and their complex) in sediment porewaters can, to some extent, contribute to the long-distance ET in the sediment columns.

In the sediment columns, redox-active species mainly existed in the solid phase. Measurements show that the EDC values in pore water contributed <12% of the ΔEDC values measured after 24 d (Table 1 and Supplementary Table 2). In the subsurface, DOC, microbes, and redox-active species are in both dissolved and solid forms (Fig. 1). Sediment Fe(II) content showed a similar variation with ΔEDC (Supplementary

https://doi.org/10.1038/s41467-024-50974-x

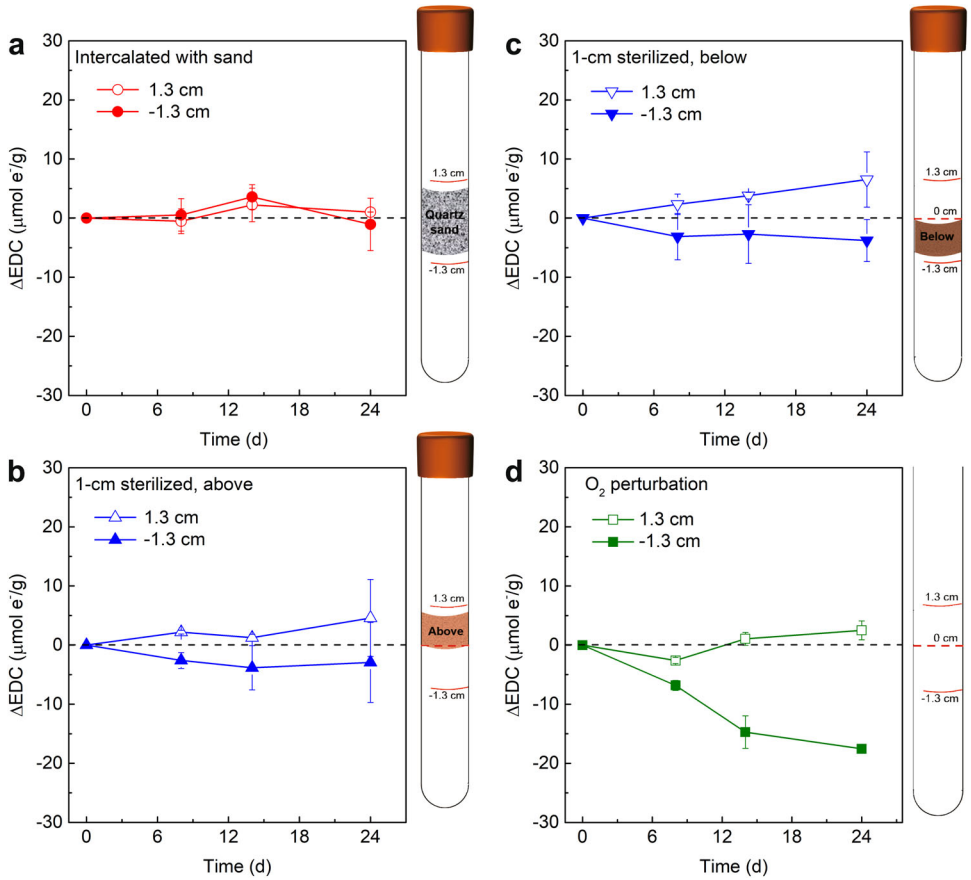

Fig. 4 | Long-distance ET in the columns with different modifications. Temporal variation of ΔEDC near the oxidized/reduced interface (locations at 1.3 and −1.3 cm) in the clay loam columns **a** with the inclusion of 2-cm thick quartz sand, **b**, **c** with the inclusion of 1-cm thick interlayer treated by concentrated $HgCl_2$ and NaN_3 above and below the interface, and **d** with the top exposed to air. "1-cm sterilized" means that a 1 cm thickness of clay loam was treated with 2 g/L $HgCl_2$ and 19.5 g/L NaN_3. The clay loam sediment (Table 1) filled in these columns was sterilized by immersing in 250 mg/L $HgCl_2$ and 500 mg/L NaN_3 prior to filling. The full schematics of these columns are displayed in Supplementary Fig. 2b, c. The photos of O_2-perturbated columns were displayed in Supplementary Fig. 19. Error bars represent standard deviations of duplicate columns (mean ± standard error, $n = 2$, independent replicates).

Figs. 10, 12d–f, and 14b). Thus, the variation of solid and aqueous redox-active species supports the 5th mechanism that we hypothesized. The redox gradient can be regarded as the driving force for the directional ET. Microbial and chemical reactions constitute the primary units of short-distance ET processes, and the directional series of many of these units constitutes the long-distance ET chain (Fig. 1). Redox-active species (i.e., NOM and Fe) in both dissolved and solid phases as well as electroactive microbes are supposed to be good candidates for developing the ET network among different redox reactions. For a sufficiently long time, the distance for the ET chain is theoretically equal to the length of a continuous redox gradient, i.e., centimeters to meters or even longer.

The favorable conditions for the occurrence of directional long-distance ET can be presumably summarized as follows. (1) A redox gradient is the prerequisite, which provides the driving force for the directional ET over a long distance. (2) Physical contact between reducers and oxidizers, either redox-active substances or microbes, is essential for the occurrence of electron hopping. (3) A higher microbial activity and more redox-active species are normally beneficial because they are the primary mediators for electron shuttling/hopping and constitute the long-distance ET network. However, when the biodegradable redox-active species such as fresh NOM are too abundant, the localized biogeochemical reactions could be intensive and screen the long-distance ET (Supplementary Section 3). (4) Diffusion of solutes in porewaters can physically mobilize electron carriers, enhancing the interaction between reducers and oxidizers and thus the long-distance ET. The distance of diffusion decreases with the decrease in matrix permeability. A strong diffusion may result in the physical movement of redox-active species, which reduces the contribution of long-distance ET.

To facilitate understanding, we summarized 3 general modes for the directional long-distance ET in the subsurface (Fig. 5). (1) Mode 1: favorable long-distance ET with abundant electron mediators and weak advection/diffusion (Fig. 5a). This mode occurs mainly in the low-permeability subsurface (i.e., clay-dominated) where redox-active components are abundant in both solid matrix and porewater but advection/diffusion is insignificant or limited. The "crowded" electron mediators allow to transfer electrons "hand-by-hand". (2) Mode 2: unfavorable long-distance ET with sparse distribution of electron mediators and strong advection/diffusion. In contrast to mode 1, this mode occurs mainly in the high-permeability subsurface (i.e., sandy habitats) where redox-active components are sparse but advection/diffusion is strong. The electron mediators cannot be connected to each other, while their dissolved form can be mobilized by advection/diffusion. In this mode, diffusion may contribute significantly. (3) Mode 3: moderate long-distance ET with moderate electron mediators and advection/diffusion. As an intermediate mode between modes 1 and 2, mode 3 mainly occurs in the moderate-permeability subsurface (i.e., silty). The electron mediators can sometimes interact and be connected each other. The short-distance mobilization due to advection/diffusion can enhance the "hand-by-hand" connection of mediators, enabling long-distance ET.

The directional long-distance ET chain provides a new perspective in understanding biogeochemical processes in the subsurface.

https://doi.org/10.1038/s41467-024-50974-x

Table 1 | Summary of column experiments and associated results

Sediment columns		Oxidized half		Reduced half	
		Initial EDC (μmol e^-/g)	Total electrons accepted within 24 d (μmol e^-/g)[a]	Initial EDC (μmol e^-/g)	Total electrons donated within 24 d (μmol e^-/g)[a]
Sand loam		2.5 ± 1.0[b]	3.5 ± 0.9	20.4 ± 3.4	3.3 ± 0.1
Silt loam		21.2 ± 3.8	10.8 ± 0.7	55.7 ± 2.4	12.1 ± 2.3
Clay loam-1	Treated by $HgCl_2$ + NaN_3 (reference)	18.5 ± 2.9	10.3 ± 2.1	48.3 ± 1.5	10.5 ± 0.4
	Inclusion of 2-cm sand	18.5 ± 2.9	\	48.3 ± 1.5	\
	Untreated	22.0 ± 3.6	18.6 ± 0.9	58.3 ± 1.5	16.7 ± 1.2
	Autoclaved	22.8 ± 0.7	9.8 ± 0.7	59.8 ± 1.9	7.5 ± 0.5
	Inclusion of 1-cm sterilized	18.5 ± 2.9	\	48.3 ± 1.5	\
	O_2 perturbation	16.5 ± 5.3	1.4 ± 0.6	48.7 ± 7.5	14.7 ± 1.5
Clay loam-2	Treated by $HgCl_2$ + NaN_3 (Clay loam-1 for reduced half)[c]	5.6 ± 2.3	16.8 ± 0.5	45.9 ± 3.6	7.0
	Untreated	4.9 ± 0.4	8.4	33.5 ± 1.3	9.3 ± 0.1
	Low-temperature perturbation	4.9 ± 0.4	1.9 ± 0.5	33.5 ± 1.3	3.0 ± 0.3
	Acid perturbation	7.0 ± 0.2	9.8 ± 0.5	39.6 ± 0.8	6.0 ± 0.5
	Base perturbation	6.8 ± 1.5	4.7 ± 0.2	33.3 ± 1.4	5.8 ± 0.1
Clay loam-3	Gamma-rays	15.4 ± 2.2	2.4 ± 0.5	46.3 ± 1.5	2.1

[a]Calculation for the amount of total electrons accepted/donated within 24 d is described in Supplementary Section 5.
[b]Data are presented as mean ± standard error.
[c]In this "$HgCl_2$ + NaN_3" column, the bottom half was filled with reduced clay loam-1, and the upper half was filled with the oxidized clay loam-2. Detailed information is described in Supplementary Section 3.

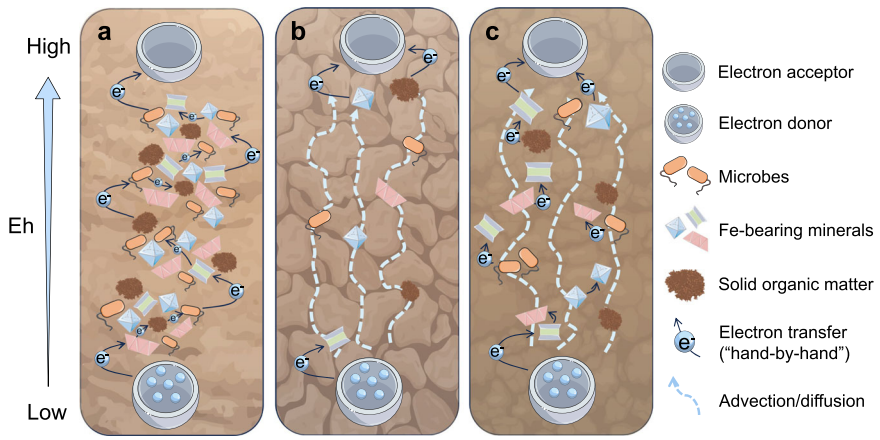

Fig. 5 | Three modes of directional long-distance ET in the subsurface. a Mode 1: favorable long-distance ET with abundant electron mediators and weak advection/diffusion. **b** Mode 2: unfavorable long-distance ET with sparse electron mediators and strong advection/diffusion. **c** Mode 3: moderate long-distance ET with moderate electron mediators and advection/diffusion.

Different scales of redox gradients occur in both natural and engineered zones in the subsurface. It has been well established that biogeochemical processes are stratified along the redox gradient, i.e., from methanogenesis to sulfate, Fe(III)/Mn(IV), nitrate, and O_2 reduction[2,11,35]. Nonetheless, it is not clear whether the ET for each of these stratified processes is directionally connected across different redox gradients. Our findings show the occurrence of a directional long-distance ET chain along the redox gradient, which connects the short-distance redox processes and functions as a hidden pathway to fuel electrons to or accept electrons from the zone over a long distance for the biogeochemical processes. To evaluate the significance of this long-distance ET chain, it is necessary to obtain the dependence of ET flux and distance on time. For the sake of simplicity, we approximately estimate the dependence of ET flux and distance on time by using the observations from the sediment columns (Supplementary Section 8). Under the initial redox gradient of ~700 mV, which can represent the near-surface soil and sediment conditions from oxidative to reductive[36,37], the rate of ET flux was 6.73 μmol e^-/(cm^2 d) (Fig. 3a), and for ET distance was 0.34 cm/d (Supplementary Fig. 21b) for the reduced half. The ET flux indicates that 6.73 μmol e^- per day can be transported from deep reduced sediments across a 1-cm^2 area to upper oxidized sediments. Based on the theoretical electron amount and reported rates for the reduction of O_2, nitrate, Mn(IV), Fe(III) or sulfate and the oxidation of methane[38–44] (Supplementary Tables 4 and 5), our estimates imply that the long-distance ET (6.73 μmol e^- cm^{-2} d^{-1}) could possibly result in comparable rates for denitrification, Fe(III) reduction, sulfate reduction, and anaerobic methane oxidation (Table 2). The rate of ET distance suggests that electrons can be transported to a distance of 0.34 cm per day. As the redox potential gradient in real environments declines with the consumption of electron acceptors/

Table 2 | Reported rates and estimated rates due to directional long-distance ET for different biogeochemical reactions

Biogeochemical reactions	Reported rates	Estimated rate by long-distance ET
Denitrification	1.41×10^{-3}–1.0 μmol NO_3^- /(cm^3·d)[38]	1.35 μmol NO_3^-/(cm^3·d)
Dissimilatory manganese reduction	4.27×10^{-4}–180 μmol Mn(IV)/(cm^3·d)[39,40]	3.37 μmol Mn(IV)/(cm^3·d)
Dissimilatory iron reduction	0–65 μmol Fe(III)/(cm^3·d)[39,41]	6.73 μmol Fe(III)/(cm^3·d)
Sulfate reduction	0.53 μmol SO_4^{2-}/(cm^3·d)[42]	0.84 μmol SO_4^{2-}/(cm^3·d)
Anaerobic methane oxidation	≥2.17×10^{-3} μmol CH_4/(cm^3·d)[43,44]	0.84 μmol CH_4/(cm^3·d)

The biogeochemical reactions include denitrification, Mn(IV) reduction, Fe(III) reduction, sulfate reduction, and anaerobic methane oxidation. "Reported rate" in previous studies was unified to the same unit of μmol/(cm^3 d) for comparison. "Estimated rate by long-distance ET" was calculated from the ET flux (6.73 μmol e^- cm^{-2} d^{-1}) and number of electrons required for different reactions (Supplementary Table 5). The details for reaction conditions are displayed in Supplementary Table 6 and Supplementary Section 8.

donors, it is currently difficult to quantitatively estimate the distance that ET can reach. Nonetheless, our results implicate that the electron sources or sinks from some distance away, i.e., >10 cm, may influence the biogeochemical processes along the redox potential gradient.

As the long-distance ET chain may also occur under extremely acidic/alkaline and cold/hot conditions, this chain could be of significance for deep-earth and deep-time processes. Perturbations by tectonic activities can develop redox gradients on a short timescale in the deep earth. For example, continental and oceanic subduction can import redox-active species into deep Earth, which perturbs the stable redox conditions and leads to the development of a new redox gradient[45,46]. The long-distance ET chain, possibly through a chemical mechanism as microbial activity is limited, may slowly transport electrons from reduced to less reduced or oxidized environments. When life is scarce on land in the deep time, reactions between land surface and atmosphere may play important roles in mediating redox conditions of both terrestrial and atmospheric environments[47,48]. With the oxygenation of the atmosphere, the reduced species like Fe(II) and S(-II) in the land surface could be oxidized by the atmospheric O_2, and thus a redox gradient could develop between the oxidized land surface and the reduced zones below the surface. As atmospheric oxygenation lasted for a long time, and the land contained abundant reduced species, this redox gradient could be sustained for a long time. We, therefore, infer that the directional long-distance ET chain may possibly have driven the oxidation front from the land surface to the zones deeper and deeper below the land surface, and the abundant "remote" electrons therein may have retarded atmospheric oxygenation through O_2 consumption in deep time.

Another insightful implication is for subsurface remediation and waste treatment. For most remediation activities, the chemicals or microbes for contaminant degradation must be injected and delivered to be in contact with the contaminants in the subsurface. This mass transfer process is a key challenge for a successful remediation[49], particularly in low-permeability aquifers. The finding of a long-distance ET chain indicates that the physical contact between chemicals or microbes and contaminants can be alleviated when a continuous redox gradient between them can be created and sustained. Provided that remediation time is not urgent, the directional long-distance ET chain can slowly sustain the redox reactions between the physically separated redox couples for contaminant transformation. For waste and wastewater treatments, long-distance ET may also occur due to the presence of redox gradient and abundant biosolids (i.e., biofilms and sludges).

Methods

Sediment column experiments

Three textures of sediments were collected from different depositional environments in Hubei province, central China. The details for sediment sampling, pretreatment, and sterilization are shown in Supplementary Section 1. The pristine sediments (E_h < −130 mV, vs. SHE, Supplementary Table 1) were used as the reduced sediments. The oxidized sediments (E_h > +420 mV) were obtained by oxygenating the pristine sediments and stored at different times (Supplementary Section 1). Polypropylene tubes (1.45 cm diameter, 10.6 cm length) were used as the sediment columns. In a typical column, the bottom half was filled with 12–15 g of reduced sediments (water content: 21.7 ± 0.1%), and the upper half was filled with the same quantity of oxidized sediments (Supplementary Fig. 2). Both the oxidized and reduced sediments had been immersed in 250 mg/L $HgCl_2$ and 500 mg/L NaN_3 prior to filling. Note that this treatment was originally performed to completely inhibit microbial activity, but later results only support an incomplete inhibition. The column was sealed immediately, wrapped tightly by aluminum foils, and placed vertically for different times (0–24 d). The column experiments were conducted in an anoxic glove box (COY, USA, 96% N_2 and 4% H_2). At different time points, two columns in parallel were sacrificed, and the sediment samples at locations 5.3, 3.9, 2.6, 1.3, −1.3, −2.6, −3.9, and −5.3 cm (relative to the oxidized/reduced interface) (Supplementary Fig. 2) were taken out within 10 min. Portions of the samples were used for the analysis of EDC, Fe(II) concentration, and amplicon sequence.

The following parameters were varied in the columns to observe the response of directional long-distance ET. (1) Sediment textures. The sediment textures included clay loam, silt loam, and sand loam (Supplementary Table 1). (2) Sediment sterilization intensity. Three sterilization methods were used to create different intensities of sterilization. These treatments include immersion in 250 mg/L $HgCl_2$ + 500 mg/L NaN_3, autoclaving for 20 min, and exposure to gamma radiation (Supplementary Section 2). (3) Inclusion of an interlayer. One interlayer is a 2-cm thick quartz sand (200 mesh) in the oxidized/reduced interface (Supplementary Fig. 2b), which aims to physically separate the oxidized and reduced sediments in the column. The quartz sand was also immersed in 250 mg/L $HgCl_2$ and 500 mg/L NaN_3 to attain the same conditions as the sediments. Another interlayer is a 1-cm thick sediment that has been harshly treated with $HgCl_2$ + NaN_3 (oxidized or reduced) filled just above or below the interface (Supplementary Fig. 2c), which aims to create a barrier when the microbial process is very weak. This sediment treatment referred to the immersion in 2 g/L $HgCl_2$ and 19.5 g/L NaN_3. (4) Sediment initial reduction potential (E_h). To investigate the impact of the initial E_h of sediments on ET, the oxidized clay loam-2 with a shorter storage time (detailed in Supplementary Section 1) and a higher initial E_h (E_h = +608.7 mV, Supplementary Table 1) was chosen to fill the upper half of the column, while the reduced clay loam-1 with an initial E_h of −257.3 mV was filled in the bottom half of the column (Supplementary Fig. 2a). Both oxidized clay loam-2 and reduced clay loam-1 were immersed in 250 mg/L $HgCl_2$ and 500 mg/L NaN_3 prior to filling. (5) Sediment temperature, pH, and E_h. The untreated clay loam-2 columns were used as reference columns to be further perturbated under different conditions. These columns were placed at ambient temperature (25 °C) or maintained at a low temperature (−20 °C) for temperature perturbation. The initial sediment pH was pH-neutral (Supplementary Table 1), and was acidified to ~4 by dilute H_2SO_4 or alkalized to ~12 by dilute NaOH for pH perturbation. The pH in the acid and base perturbated columns varied from ~4 to 6.4 and from ~12 to 8.9 within 24 d, respectively (Supplementary Fig. 17). To adjust the redox gradient during the ET process, the column was moved out from the anoxic

glove box, and the top of oxidized half was uncovered and exposed to air for O_2 perturbation. To avoid cracks due to drying, 20–46-µL deionized water was added to the top every day. The initial EDC values of sediments in the above columns under different conditions are summarized in Table 1.

EDC and EAC analysis

Mediated electrochemical analysis has been successfully applied to quantify the redox properties of Fe-bearing minerals and particulate NOM in sediments[19–21], and also to evaluate microbially catalyzed NOM redox cycling in both laboratory pure cultures and freshwater sediments[19,21]. In this study, mediated electrochemical oxidation (MEO) and reduction (MER) were applied to quantify the EDC and EAC of sediments and sediment pore waters in the main experiments. A glassy carbon cell was used as the working electrode, an Ag/AgCl as the reference electrode, and a coiled platinum wire as the auxiliary electrode. The electrochemical measurements were controlled by a CHI1000C electrochemical workstation (Shanghai CH Instruments, China). The electrolyte solution contained 0.1 M KCl at pH 7.1 buffered by 0.01 M MOPS (3-(Nmorpholino)propanesulfonic acid). 2,2′-azino-bis(3-ethylbenzothiazoline-6-sulfonic acid) (ABTS) and ethyl viologen dibromide (EtV) were used as the electron transfer mediators in MEO and MER measurements, respectively[19]. MEO was carried out under anoxic conditions and the electrode was equilibrated at the desired potential (0.61 V vs. SHE)[50]. MER was carried out inside the anoxic glove box to avoid O_2 oxidation, and the electrode was equilibrated at −0.45 V (vs. SHE)[19]. The final concentrations of ABTS and EtV were both 125 µM in 40 mL of electrolyte solution. EDC or EAC was obtained by integration of the current peaks. The detection limits for MEO and MER are 2.3 and 25.2 nmol electrons transferred between the sample, mediator, and electrode, respectively. For solid phase sample measurement, 0.1–3 mg of sediments were added to the glassy carbon cell, and for the aqueous phase sample, 1–5 mL of dilute pore water samples were in the glassy carbon cell.

The EDC values of sediments in the sand loam, pH, and temperature-perturbated columns were measured by spectrophotometry. According to previous studies[51–53], the EDC of samples was analyzed by quantifying the difference of $ABTS^{\bullet-}$ concentration before and after oxidation with the sample. Before testing the samples, $ABTS^{2-}$ was oxidized to $ABTS^{\bullet-}$ by $Na_2S_2O_8$ at a molar ratio of 2:1 at 50 °C for 2 h. Subsequently, the residual $Na_2S_2O_8$ was removed by 0.01 M $FeSO_4$ (pH = 1), and the pH was adjusted to 6.9 using 1 M NaOH and 0.01 M MOPS (pH = 6.9). Finally, the solution was filtered through a 0.45-µm membrane, and the $ABTS^{\bullet-}$ filtrate was collected and stored at 4 °C. About 0.1 g sediment sample was reacted with 10-mL 0.6–8.6 µmol of $ABTS^{\bullet-}$ for 10 min, which had been deoxygenated by N_2. The absorbances of $ABTS^{\bullet-}$ before and after the reaction were measured at 734 nm using a UV spectrophotometer. The concentration of reduced $ABTS^{\bullet-}$ in the sample was further calculated based on the molar absorptivity ($\varepsilon = 1.5 \times 10^4\ M^{-1}\ cm^{-1}$ at 734 nm)[54], which was equal to the EDC values of the sediment sample. The detection limit for the electron transfer between the sample and $ABTS^{\bullet-}$ is 77.0 nmol.

Fe and DOC measurement

The Fe(II) in sediment samples including dissolved Fe^{2+} and Fe(II) in solids was quantified by the 1,10-*o*-phenanyhroline analytical method[55]. In detail, ~200-mg sediment samples were extracted by 4.8-mL 3.6 M H_2SO_4 and 0.6-mL 40% HF for 24 h. The dissolved solution was mixed with 0.1 M H_3BO_3 in equal volume and was then added to 0.5% 1,10-*o*-phenanyhroline. The absorbance was determined at a wavelength of 510 nm.

At different sampling time, the sediment suspension samples were collected, and supernatant samples in the suspensions were separated by filtrating through a 0.45-µm membrane. The dissolved organic carbon (DOC) was determined by a TOC analyzer (Shimadzu TOC-L CPH).

Water-extracted solutes and estimated concentrations in pore water

The required sediment pore water cannot be collected directly because of the small sediment volume. Instead, we thoroughly mixed sediment samples with water at a soil:water ratio of around 1:20, and then separated the water by a 0.45-µm membrane. The dissolved species contents were measured as water-extracted concentrations which were unified to each gram of wet sediment.

The estimation of dissolved species content in pore water involves several steps. First, the mass of pore water in the sediment sample was determined based on the water content (Supplementary Table 1). The volume of pore water was further acquired by assuming the pore water density to be 1 g/mL. Then, the water-extracted concentrations of different dissolved species were measured. The ratio of the added water volume to the pore water volume was used as a dilution factor. At last, the concentration of dissolved species in the sediment pore water was calculated based on the dilution factor. The water-extracted and estimated solute concentrations of the sediment pore waters in the columns were displayed in Supplementary Tables 2 and 3. It should be noted that this means can overestimate the solute concentrations in sediment pore waters because of the much larger water volume. So, this value was only used to represent the existence of solutes in sediment pore waters.

Nucleic acid extraction, cDNA synthesis, and quantitative PCR

In order to estimate the microbial abundance in the sediments after different sterilization treatments and temperature/pH perturbations, the abundance of 16S rRNA genes (RNA-based) was quantified by incubating oxidized clay loam-2 for 24 h under different conditions: 5 g of oxidized clay loams were incubated separately by 10 mL of 250 mg/L $HgCl_2$ and 500 mg/L NaN_3 ("$HgCl_2 + NaN_3$") solution, concentrated $HgCl_2$ (2 g/L) and NaN_3 (19.5 g/L) mixed solution ("Concentrated $HgCl_2 + NaN_3$"), dilute H_2SO_4 ("Acid perturbation"), dilute NaOH ("Base perturbation") or sterile deionized water ("Untreated"). The above sediment suspensions were incubated in a shaking incubator (25 ± 2 °C, 220 rpm) for 24 h. For autoclaving, 5 g of oxidized clay loam was autoclaved at 121 °C for 20 min (1.5 h for the whole process) and mixed with 10 mL of sterile deionized water and then incubated at 25 ± 2 °C, 220 rpm for ~22.5 h ("Autoclaved"). For gamma radiation, 5 g of oxidized clay loam was mixed with 10 mL of deionized water and then exposed to a cobalt60 radiation field and radiated by a dose of 52 ± 5.2 kGy for 13 h ("Gamma-rays"). For temperature perturbation, 5 g of oxidized clay loam was mixed with 10 mL of sterile deionized water and then the suspension was maintained at a low temperature (−20 °C) for 24 h ("Low temperature").

The above suspensions were centrifuged at 7500 *g* for 2 min (4 °C) to obtain sediment samples. RNA was extracted from sediment samples using the RNeasy PowerSoil Total RNA (Qiagen, Hilden, Germany) kits, following the manufacturer's instructions. The quality and quantity of RNA were examined using a NanoDrop-2000 spectrophotometer (Thermo Fisher Scientific, Waltham, MA, USA) and agarose (1%) (Biowest, Riverside, MO, USA) gel electrophoresis. To ensure DNA removal, the RNA extracts were treated with Recombinant DNase I (TaKaRa Bio) as directed by the manufacturer. Then cDNA was synthesized using a PrimeScript™ II 1st Strand cDNA Synthesis Kit (TaKaRa Bio) and was stored at −20 °C for quantitative analysis. The abundance of 16S rRNA genes (V4 region) (RNA-based) was further performed in triplicate. For qPCR analysis, the bacterial 16S rRNA genes were amplified with the primers 515F (5′-GTGCCAGCMGCCGCGGTAA-3′) and 806R (5′-GGACTACHVGGGTWTCTAAT-3′). The reaction was performed using TB Green Premix Ex Taq™ II (Tli RNaseH Plus) on a LightCycler PCR instrument (LC96, Roche, Switzerland). The reaction mixture used for each qPCR comprised 10 µL of TB Green Premix Ex Taq II (Tli RNaseH Plus) (2×), 0.8 µL each of forward and reverse primers (10 µM), 2 µL of cDNA, and 6.4 µL of nuclease-free

water and the total volume was 20 µL. The qPCR cycling was set as follows: 95 °C for 30 s; 40 cycles of 95 °C for 30 s, 60 °C for 30 s and 72 °C for 60 s. Plasmids were extracted from *Escherichia coli* DH5α hosts using the MiniBEST Plasmid Purification Kit (TaKaRa Bio). The calibration curve for the 16S rRNA gene copies was made using 10-fold serial dilutions of the plasmids, and amplification efficiency was 95% with R^2 higher than 0.99. The absolute abundance of 16S rRNA genes was shown as gene copy numbers per gram of wet sediment.

After different treatments for 24 h, compared with untreated sediment samples, the RNA-based 16S rRNA genes abundance decreased by 2 and 4 orders of magnitude in the sediment samples from "$HgCl_2 + NaN_3$" to "Concentrated $HgCl_2 + NaN_3$", and decreased to below detection limit in the sediment samples from "Autoclaved" and "Gamma-rays" (Supplementary Fig. 3). These results indicate the sequence of decreased microbial abundance in different sterilized sediments. Besides, the RNA-based 16S rRNA genes abundance decreased by 3 and 2 orders of magnitude for temperature and pH perturbations, respectively (Supplementary Fig. 3), which also implies the weak microbial activity in different perturbated sediments especially in the "Low temperature" sediment.

PCR amplification analysis

For the amplicon sequencing analysis, sediment DNA was extracted by MagaBio Soil/Feces Genomic DNA Purification Kit (Guangdong Magigene Biotechnology Co., Ltd., China).16S rRNA genes (V3-V4 region) were amplified by TaKaRa Premix Taq Version 2.0 (TaKaRa Biotechnology Co., Dalian, China) with the primer set of 338F (5′-ACTCC TACGGGAGGCAGCA-3′) and 806R (5′-GGACTACHVGGGTWTCTAAT-3′) for different sediment samples. Sample-specific 470-bp barcodes were incorporated into the primers for multiplex sequencing. The reaction mixture used for each PCR comprised 25 µL of 2x Premix Taq, 1 µL each of forward and reverse primers (10 µmol/L), 50 ng of DNA, and 50 µL of nuclease-free water, and the total volume was 50 µL. The PCR conditions were as follows: 94 °C for 5 min; 33 cycles of denaturation at 94 °C for 30 s and annealing at 52 °C for 30 s and extension at 72 °C for 30 s; and a final extension at 72 °C for 8 min.

Sequencing and data analysis

The PCR products of these samples were equally mixed and purified and prepared for paired-end sequencing on the Illumina Novaseq 6000 platform at Guangdong Magigene Biotechnology Co., Ltd.[56,57]. The sequence data were deposited into the NCBI's Sequence Read Archive Database with accession numbers PRJNA949398. Three replicates were performed for each sample in qPCR and amplicon sequencing analysis. The Non-singleton amplicon sequence variants (ASVs) with 100% sequence similarity screened by the Unoise3 method were annotated by Silva 132 database[58–60].

Reporting summary

Further information on research design is available in the Nature Portfolio Reporting Summary linked to this article.

Data availability

Sequence data are available in NCBI (BioProject PRJNA949398). The data generated in this study have been deposited in Dryad under the accession code (https://doi.org/10.5061/dryad.xd2547dq8) and are also provided in the Supplementary Information.

References

1. Peiffer, S. et al. A biogeochemical–hydrological framework for the role of redox-active compounds in aquatic systems. *Nat. Geosci.* **14**, 264–272 (2021).
2. Borch, T. et al. Biogeochemical redox processes and their impact on contaminant dynamics. *Environ. Sci. Technol.* **44**, 15–23 (2010).
3. Chen, K. et al. Vertical hydrologic exchange flows control methane emissions from riverbed sediments. *Environ. Sci. Technol.* **57**, 4014–4026 (2023).
4. Yanina, S. V. & Rosso, K. M. Linked reactivity at mineral-water interfaces through bulk crystal conduction. *Science* **320**, 218–222 (2008).
5. Lovley, D. R. Syntrophy goes electric: direct interspecies electron transfer. *Annu. Rev. Microbiol.* **71**, 643–664 (2017).
6. Shi, L. et al. Extracellular electron transfer mechanisms between microorganisms and minerals. *Nat. Rev. Microbiol.* **14**, 651–662 (2016).
7. Malvankar, N. S., King, G. M. & Lovley, D. R. Centimeter-long electron transport in marine sediments via conductive minerals. *ISME J.* **9**, 527–531 (2015).
8. Kato, S., Hashimoto, K. & Watanabe, K. Microbial interspecies electron transfer via electric currents through conductive minerals. *Proc. Natl Acad. Sci. USA* **109**, 10042–10046 (2012).
9. Pfeffer, C. et al. Filamentous bacteria transport electrons over centimetre distances. *Nature* **491**, 218–221 (2012).
10. Bai, Y. et al. AQDS and redox-active NOM enables microbial Fe(III)-mineral reduction at cm-scales. *Environ. Sci. Technol.* **54**, 4131–4139 (2020).
11. Kappler, A. et al. An evolving view on biogeochemical cycling of iron. *Nat. Rev. Microbiol.* **19**, 360–374 (2021).
12. Boland, D. D., Collins, R. N., Miller, C. J., Glover, C. J. & Waite, T. D. Effect of solution and solid-phase conditions on the Fe(II)-accelerated transformation of ferrihydrite to lepidocrocite and goethite. *Environ. Sci. Technol.* **48**, 5477–5485 (2014).
13. Ma, D., Wu, J., Yang, P. & Zhu, M. Coupled manganese redox cycling and organic carbon degradation on mineral surfaces. *Environ. Sci. Technol.* **54**, 8801–8810 (2020).
14. Chen, C., Hall, S. J., Coward, E. & Thompson, A. Iron-mediated organic matter decomposition in humid soils can counteract protection. *Nat. Commun.* **11**, 2255 (2020).
15. Qian, A. et al. Mechanistic insight into electron transfer from Fe(II)-bearing clay minerals to Fe (hydr)oxides. *Environ. Sci. Technol.* **57**, 8015–8025 (2023).
16. Klüpfel, L., Piepenbrock, A., Kappler, A. & Sander, M. Humic substances as fully regenerable electron acceptors in recurrently anoxic environments. *Nat. Geosci.* **7**, 195–200 (2014).
17. Melton, E. D., Swanner, E. D., Behrens, S., Schmidt, C. & Kappler, A. The interplay of microbially mediated and abiotic reactions in the biogeochemical Fe cycle. *Nat. Rev. Microbiol.* **12**, 797–808 (2014).
18. Aeschbacher, M., Sander, M. & Schwarzenbach, R. P. Novel electrochemical approach to assess the redox properties of humic substances. *Environ. Sci. Technol.* **44**, 87–93 (2010).
19. Sander, M., Hofstetter, T. B. & Gorski, C. A. Electrochemical analyses of redox-active iron minerals: a review of nonmediated and mediated approaches. *Environ. Sci. Technol.* **49**, 5862–5878 (2015).
20. Lau, M. P., Sander, M., Gelbrecht, J. & Hupfer, M. Solid phases as important electron acceptors in freshwater organic sediments. *Biogeochemistry* **123**, 49–61 (2015).
21. Gao, C., Sander, M., Agethen, S. & Knorr, K.-H. Electron accepting capacity of dissolved and particulate organic matter control CO_2 and CH_4 formation in peat soils. *Geochim. Cosmochim. Acta* **245**, 266–277 (2019).
22. McNamara, N. P., Black, H. I. J., Beresford, N. A. & Parekh, N. R. Effects of acute gamma irradiation on chemical, physical and biological properties of soils. *Appl. Soil Ecol.* **24**, 117–132 (2003).
23. Otte, J. M. et al. Sterilization impacts on marine sediment—āre we able to inactivate microorganims in environmental samples? *FEMS Microbiol. Ecol.* **94**, fiy189 (2018).
24. Huang, J. Z. et al. Fe(II) redox chemistry in the environment. *Chem. Rev.* **121**, 8161–8233 (2021).
25. Mooshammer, M. et al. Decoupling of microbial carbon, nitrogen, and phosphorus cycling in response to extreme temperature events. *Sci. Adv.* **3**, e1602781 (2017).

26. Fierer, N. Embracing the unknown: disentangling the complexities of the soil microbiome. *Nat. Rev. Microbiol.* **15**, 579–590 (2017).
27. Karhu, K. et al. Temperature sensitivity of soil respiration rates enhanced by microbial community response. *Nature* **513**, 81–84 (2014).
28. Price, P. B. & Sowers, T. Temperature dependence of metabolic rates for microbial growth, maintenance, and survival. *Proc. Natl Acad. Sci. USA* **101**, 4631–4636 (2004).
29. Rousk, J., Brookes, P. C., & Bååth, E. Contrasting soil pH effects on fungal and bacterial growth suggest functional redundancy in carbon mineralization. *Appl. Environ. Microbiol.* **75**, 1589–1596 (2009).
30. Yabusaki, S. B. et al. Water table dynamics and biogeochemical cycling in a shallow, variably-saturated floodplain. *Environ. Sci. Technol.* **51**, 3307–3317 (2017).
31. Wei, M. et al. Denitrification mechanism in oxygen-rich aquatic environments through long-distance electron transfer. *npj Clean Water* **5**, 61 (2022).
32. Reddy, K. R., Patrick, W. H. & Broadbent, F. E. Nitrogen transformations and loss in flooded soils and sediments. *Crit. Rev. Environ. Sci. Technol.* **13**, 273–309 (1984).
33. Dong, H. et al. Coupled iron cycling and organic matter transformation across redox interfaces. *Nat. Rev. Earth Environ.* **4**, 659–673 (2023).
34. Bai, Y. et al. Networks of dissolved organic matter and organo-mineral associations stimulate electron transfer over centimeter distances. *Environ. Sci. Technol. Lett.* **10**, 493–498 (2023).
35. Gandy, C. J., Smith, J. W. N. & Jarvis, A. P. Attenuation of mining-derived pollutants in the hyporheic zone: a review. *Sci. Total Environ.* **373**, 435–446 (2007).
36. Rinklebe, J., Shaheen, S. M. & Yu, K. Release of As, Ba, Cd, Cu, Pb, and Sr under pre-definite redox conditions in different rice paddy soils originating from the U.S.A. and Asia. *Geoderma* **270**, 21–32 (2016).
37. Chen, C., Kukkadapu, R. K., Lazareva, O. & Sparks, D. L. Solid-phase Fe speciation along the vertical redox gradients in floodplains using XAS and Mössbauer spectroscopies. *Environ. Sci. Technol.* **51**, 7903–7912 (2017).
38. Pan, H. et al. Dissimilatory nitrate/nitrite reduction to ammonium (DNRA) pathway dominates nitrate reduction processes in rhizosphere and non-rhizosphere of four fertilized farmland soil. *Environ. Res.* **186**, 109612 (2020).
39. Canfield, D. E., Kristensen, E. & Thamdrup, B. The iron and manganese cycles. in *Adv. Mar. Biol.* (Academic Press, 2005) pp. 269–312.
40. Bandstra, J. Z., Ross, D. E., Brantley, S. L. & Burgos, W. D. Compendium and synthesis of bacterial manganese reduction rates. *Geochim. Cosmochim. Acta* **75**, 337–351 (2011).
41. Bonneville, S., Cappellen, P. V. & Behrends, T. Microbial reduction of iron(III) oxyhydroxides: effects of mineral solubility and availability. *Chem. Geol.* **212**, 255–268 (2004).
42. Findlay, A. J., Pellerin, A., Laufer, K. & Jørgensen, B. B. Quantification of sulphide oxidation rates in marine sediment. *Geochim. Cosmochim. Acta* **280**, 441–452 (2020).
43. Egger, M., Riedinger, N., Mogollón, J. M. & Jørgensen, B. B. Global diffusive fluxes of methane in marine sediments. *Nat. Geosci.* **11**, 421–425 (2018).
44. Scheller, S., Yu, H., Chadwick, G. L., McGlynn, S. E. & Orphan, V. J. Artificial electron acceptors decouple archaeal methane oxidation from sulfate reduction. *Science* **351**, 703–707 (2016).
45. Cannaò, E. & Malaspina, N. From oceanic to continental subduction: Implications for the geochemical and redox evolution of the supra-subduction mantle. *Geosphere* **14**, 2311–2336 (2018).
46. Ge, R.-F., Wilde, S. A., Zhu, W.-B. & Wang, X.-L. Earth's early continental crust formed from wet and oxidizing arc magmas. *Nature* **623**, 334–339 (2023).
47. Muller, É., Philippot, P., Rollion-Bard, C. & Cartigny, P. Multiple sulfur-isotope signatures in Archean sulfates and their implications for the chemistry and dynamics of the early atmosphere. *Proc. Natl Acad. Sci. USA* **113**, 7432–7437 (2016).
48. Daines, S. J., Mills, B. J. W. & Lenton, T. M. Atmospheric oxygen regulation at low Proterozoic levels by incomplete oxidative weathering of sedimentary organic carbon. *Nat. Commun.* **8**, 14379 (2017).
49. Yuan, Y., Zhou, L., Hou, R., Wang, Y. & Zhou, S. Centimeter-long microbial electron transport for bioremediation applications. *Trends Biotechnol* **39**, 181–193 (2021).
50. Aeschbacher, M., Graf, C., Schwarzenbach, R. P. & Sander, M. Antioxidant properties of humic substances. *Environ. Sci. Technol.* **46**, 4916–4925 (2012).
51. Page, S. E. et al. Dark formation of hydroxyl radical in arctic soil and surface waters. *Environ. Sci. Technol.* **47**, 12860–12867 (2013).
52. Zhang, Y. et al. Effect of C/Fe molar ratio on H_2O_2 and •OH production during oxygenation of Fe(II)-humic acid coexisting systems. *Environ. Sci. Technol.* **56**, 13408–13418 (2022).
53. Shi, C. et al. Electrokinetic-enhanced bioremediation of trichloroethylene-contaminated low-permeability soils: mechanistic insight from spatio-temporal variations of indigenous microbial community and biodehalogenation activity. *Environ. Sci. Technol.* **57**, 5046–5055 (2023).
54. Re, R. et al. Antioxidant activity applying an improved ABTS radical cation decolorization assay. *Free Radical Biol. Med.* **26**, 1231–1237 (1999).
55. Amonette, J. E. & Templeton, J. C. Improvements to the quantitative assay of nonrefractory minerals for Fe(II) and total Fe using 1,10-phenanthroline. *Clays Clay Miner* **46**, 51–62 (1998).
56. Kozich, J. J., Westcott, S. L., Baxter, N. T., Highlander, S. K. & Schloss, P. D. Development of a dual-index sequencing strategy and curation pipeline for analyzing amplicon sequence data on the MiSeq Illumina Sequencing Platform. *Appl. Environ. Microbiol.* **79**, 5112–5120 (2013).
57. Ju, F., Lau, F. & Zhang, T. Linking microbial community, environmental variables, and methanogenesis in anaerobic biogas digesters of chemically enhanced primary treatment sludge. *Environ. Sci. Technol.* **51**, 3982–3992 (2017).
58. Edgar, R. C. Search and clustering orders of magnitude faster than BLAST. *Bioinformatics* **26**, 2460–2461 (2010).
59. Quast, C. et al. The SILVA ribosomal RNA gene database project: improved data processing and web-based tools. *Nucleic Acids Res.* **41**, D590–D596 (2013).
60. Huang, Y. et al. High-throughput microbial culturomics using automation and machine learning. *Nat. Biotechnol.* **41**, 1424–1433 (2023).

Acknowledgements

This work was supported by the Natural Science Foundation of China Nos. 42025703 and 42277072; National Key Technology Research and Development Program of China (2022YFC3701403). We are grateful for the discussion with Xin Wang at Nankai University on microbial extracellular ET and with Haijun Song at China University of Geosciences (Wuhan) on the significance of long-distance ET, particularly in geological history.

Author contributions

S. Y., Y. Z., and M. T. designed the research. Y. L. and P. Z. supported the methodology for EDC and EAC analysis. Y. Z. performed most of the experiments. F. Z. and Z. W. participated in the sample analyses in the sediment column experiments. P. L. helped to design qPCR and amplicon sequence analysis for sediment samples. Y. Z., S. Y., M. T., and P. Z. performed data analysis. Y. Z. and S. Y. wrote and revised the paper. A. K., P. L., and Y. W. reviewed and edited the paper. S. Y. and M. T. funded the research.

Competing interests

The authors declare no competing interests.

Additional information

Supplementary information The online version contains supplementary material available at https://doi.org/10.1038/s41467-024-50974-x.

Correspondence and requests for materials should be addressed to Songhu Yuan.

Peer review information *Nature Communications* thanks Elisa Pellegrini and the other, anonymous, reviewer for their contribution to the peer review of this work. A peer review file is available.